

Numerical study of induced current perturbations in the vicinity of excitable cells exposed to extremely low frequency magnetic fields

Noha Hassan¹, Indira Chatterjee², Nelson G Publicover¹
and Gale L Craviso³

¹ Biomedical Engineering Graduate Program, University of Nevada, Reno, NV 89557, USA

² Department of Electrical Engineering, University of Nevada, Reno, NV 89557, USA

³ Department of Pharmacology, University of Nevada, Reno, NV 89557, USA

E-mail: indira@engr.unr.edu

Received 20 March 2003, in final form 20 June 2003

Published 30 September 2003

Online at stacks.iop.org/PMB/48/3277

Abstract

Realistic three-dimensional cell morphologies were modelled to determine the current density induced in excitable cell culture preparations exposed to 60 Hz magnetic fields and to identify important factors that can influence the responses of cells to these fields. Cell morphologies representing single spherical adrenal chromaffin cells, single elongated smooth muscle cells and chromaffin cell aggregates in a Petri dish containing culture medium were modelled using the finite element method. The computations for a spherical cell revealed alterations in the magnitude and spatial distribution of the induced current density in the immediate vicinity of the cell. Maxima occurred at the equatorial sides and minima at the poles. Proximity of cells to each other as well as cell aggregate shape, size and orientation with respect to the induced current influenced the magnitude and spatial distribution of the induced current density. For an elongated cell, effects on the induced current density were highly dependent on cell orientation with respect to the direction of the induced current. These results provide novel insights into the perturbations in induced current that occur in excitable cell culture preparations and lay a foundation for understanding the mechanisms of interaction with extremely low frequency magnetic fields at the tissue level.

(Some figures in this article are in colour only in the electronic version)

1. Introduction

Interest in the interaction of extremely low frequency (ELF) magnetic fields (MFs) with living organisms has been motivated not only by reports of MF-induced physiologic effects such as alterations in heart rate and evoked brain potentials (Graham *et al* 1994), and suppression of

nocturnal pineal melatonin synthesis (Kato *et al* 1994), but also by concerns of possible human health hazards due to powerline frequency (50/60 Hz) MF exposure such as an increased incidence of childhood leukemia (Wertheimer and Leeper 1979). In addition, the successful clinical applications of time-varying MFs for stimulating nerve regeneration (Kanje *et al* 1993), accelerating bone fracture healing (Pilla 1993) and stimulating neuronal brain activity (Ueno *et al* 1988) have provided incentives for developing additional therapeutic approaches using ELF-MFs.

Attempts to provide a basic understanding of how ELF-MFs interact with humans and animals to cause biological effects have relied on a variety of *in vitro* model systems. The use of cultured cells, for example, has resulted in many reports demonstrating that cellular functions, including changes in growth rate (Tenforde 1993), gene expression (Tenforde 1996), protein synthesis (Goodman and Henderson 1991, Goodman *et al* 1995) and cell proliferation (Morgan 1989) are altered by ELF-MFs. To explain such changes in cellular function, the general consensus has been that the interaction of ELF-MFs with biological systems occurs through MF-induced electric fields and currents (Liburdy 1995, Luben 1991, Tenforde 1991). Consequently, a considerable amount of effort has been directed at characterizing the electric fields and currents induced in cultured cell model systems by time-varying MFs.

Analytical methods were first used to compute the magnitude and distribution of MF-induced electric fields and currents in both circular and rectangular cell culture dishes that contained medium with no cells present (McLeod *et al* 1983, Misakian *et al* 1993). The induced electric fields and currents were found to be dependent on the shape of the culture dish as well as the orientation (i.e., vertical or horizontal) of the MF with respect to the base of the dish. Subsequent numerical studies examined how the presence of cells perturbs the spatial distribution of induced currents. Stuchly and Xi (1994) used the three-dimensional (3D) impedance method to compute the average MF-induced electric fields and currents in a culture medium placed in a Petri dish and containing cubical-shaped cells arranged either randomly or as a confluent monolayer of cells connected by gap junctions. The results indicated that the spatial distribution of the induced current in the medium is the same as in the absence of the cells when the cells are randomly distributed throughout the dish and not touching (cell density 17%). However, when the cells are in contact with each other in a monolayer (cell density 34%), perturbations in the spatial distribution of the induced current are observed. These results point to the density of the cells as well as their position in the culture dish being important factors that determine the distribution of the induced current that the cells are exposed to. Hart (1996) reported similar results when a simplified two-dimensional model of square-shaped cells in a Petri dish was exposed to ELF-MFs. While these results provided insights into the macroscopic effects on induced currents due to the presence of cells, knowledge of the microscopic induced current changes in the close vicinity of the cells is still lacking.

Because the uniformity of electric fields and currents induced in a cell culture dish containing medium by time-varying MFs is perturbed by the presence of cells, a detailed description and quantification of the perturbations as well as identification of parameters that affect the perturbations is essential for drawing valid conclusions regarding observed cellular effects of MF exposure of cells in culture dishes. Our laboratory has been studying the effect of 60 Hz MFs on intracellular calcium levels in cultured chromaffin cells (Craviso *et al* 2002). The present numerical modelling study extends those studies by determining the magnitude and spatial distribution of the induced electric fields and currents in the immediate vicinity of the cells during 60 Hz MF-exposure. Computations were performed for realistic 3D single-cell/cell-aggregate models in a cell culture medium contained in a Petri dish, using the finite element method. This method has the advantage over the 3D impedance method

previously used by Stuchly and Xi (1994) in that cell shapes are not restricted to simple cubical models. In addition, the MF exposure system used in the computations was based on the actual experimental setup used for examining 60 Hz MF effects on intracellular calcium levels. The specific parameters that were investigated are representative of those relevant to MF exposure of cells in culture dishes in general and include cell and cell aggregate shape, cell aggregate size, spatial position of individual cells in the Petri dish, proximity of neighbouring cells and cell orientation with respect to the induced current density.

2. Computational methods

The time-varying or eddy current solver module of a commercially available finite element software package Maxwell[®] 3D Field Simulator (Ansoft Corporation, Pittsburgh, PA) was used to solve Maxwell's equations for computing the spatial distribution of the induced electric field and current density in a Petri dish containing culture medium with cells, exposed to 60 Hz MFs. The Maxwell 3D solver takes into account the geometry being modelled, electrical and magnetic properties such as dielectric constant, electrical conductivity and magnetic permeability, sources of ac magnetic fields, and the appropriate boundary conditions describing the field behaviour. The finite element method was used to divide the geometry into a mesh consisting of thousands of tetrahedral elements of various sizes. This method is very well suited for accurate modelling of simple shapes like those of isolated cells, as well as for modelling more complicated shapes such as cell aggregates. The technique uses second-order quadratic polynomials to approximate electromagnetic (EM) field quantities in each tetrahedral element and computes these quantities by minimizing an energy functional (Users Reference 1993). If the EM field solution for an element in the mesh is not within a user specified percentage error, the software further subdivides that element into smaller elements and again generates a field solution for these smaller elements. In this manner, the mesh is repeatedly refined until the solution reaches the required accuracy.

2.1. Magnetic field exposure system

The Maxwell 3D[®] field simulator was also used to construct an accurate finite element model of a MF exposure system consisting of a Helmholtz coil pair, separated by a distance of 5 cm (equal to the radius of the coils). The exposure system was based on one used in our laboratory to generate a magnetic flux density of up to 5 Gauss with a 35 mm Petri dish placed in the central plane midway between the coils (Craviso *et al* 2002). A schematic of the exposure system is shown in figure 1. The direction of current flow in both coils was the same, resulting in a uniform magnetic flux density in the central region between the coils, perpendicular to the base of the Petri dish (Misakian *et al* 1993, Mcleod *et al* 1983, Bassen *et al* 1992).

2.2. Cell models

Two types of excitable cells placed in a culture medium and exposed to a 5 Gauss, 60 Hz MF were modelled, adrenal medullary chromaffin cells and smooth muscle cells. In each case, photomicrographs of the cells (figure 2) were used as the basis for constructing realistic cell models. Since chromaffin cells are spherical in shape (figure 2(a)), they were modelled as 20 μm diameter spheres, surrounded by a 20 nm thickness cell membrane (figure 2(b)). Because chromaffin cells in culture tend to form aggregates of various sizes and shapes, realistic cell aggregates ranging from two cells to six cells were also modelled.

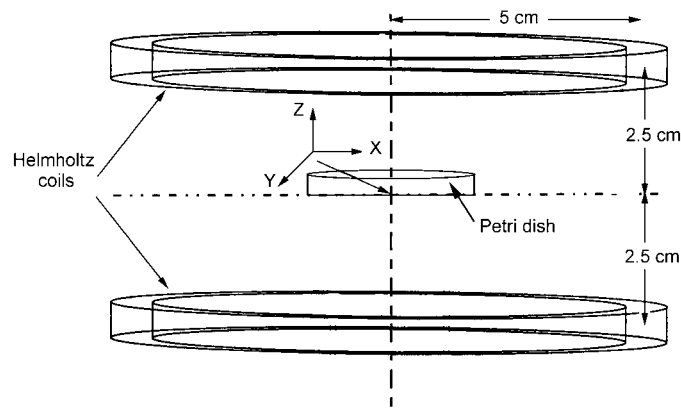


Figure 1. A schematic diagram of a Helmholtz coil pair and a Petri dish (35 mm) placed at the central plane between the coils.

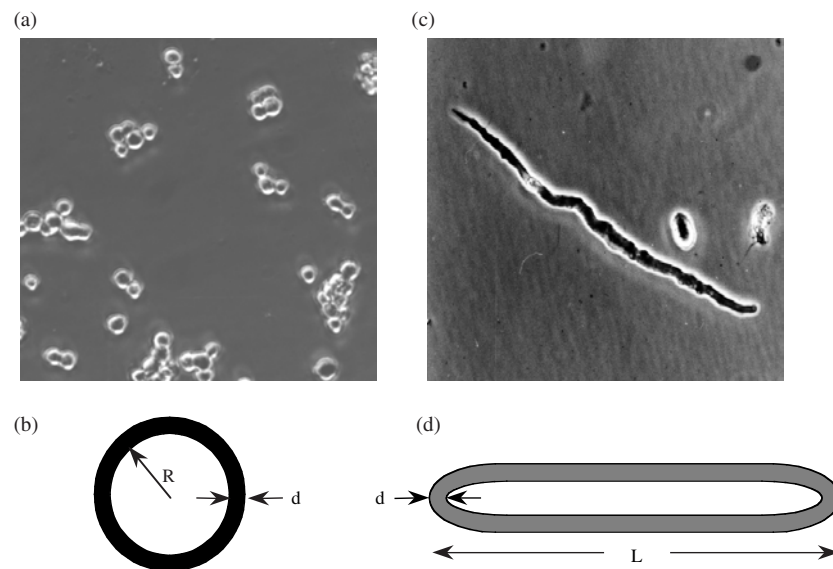


Figure 2. Photomicrographs and schematic diagrams of modelled cells. (a) Cultured chromaffin cells, (b) spherical chromaffin cell model (radius (R) = 10 μm , membrane thickness (d) = 20 nm), (c) cultured smooth muscle cell, (d) elongated smooth muscle cell model (length (L) = 100 μm , membrane thickness (d) = 20 nm).

The second cell type, smooth muscle cells, isolated from the gastrointestinal tract, are elongated with tapered ends (figure 2(c)). These cells were modelled as cylinders (100 μm in length and 5 μm in diameter) with smoothed end caps, as shown in figure 2(d), surrounded by a 20 nm thickness membrane. The values of the relative dielectric constant ϵ_r , and electrical conductivity σ of the intracellular medium, cell membrane, and extracellular medium assumed in the computations are summarized in table 1. The large differences between the dimensions of the cells (20 μm diameter for chromaffin cells and 100 μm length for smooth muscle cells),

Table 1. Relative dielectric constant ϵ_r and electrical conductivity σ of the intracellular medium, extracellular medium and cell membrane (Bassen *et al* 1992, Foster *et al* 1989).

	ϵ_r	σ (S m ⁻¹)
Intracellular medium	80	0.5
Extracellular medium	80	1.5
Cell membrane	11.3	10 ⁻⁷

the thickness of the cell membrane (20 nm) and the size of the Petri dish (35 mm) in which the cells were placed caused an aspect ratio (i.e. largest dimension/smallest dimension) problem during the numerical computations that led to a convergence error in the solution. To avoid this problem and to make the meshing process easier, the assumed value of the cell membrane thickness (20 nm) was chosen to be larger than realistic values (~5 nm) measured for biological membranes. A thicker cell membrane reduced the model complexity and computational time significantly. Virtual objects (dummy objects placed between the cells and the edges of the Petri dish and having the same material properties as the cell culture medium) were also used in the modelling process to introduce more points (i.e., tetrahedral vertices) between the objects being modelled. This strategy greatly improved the aspect ratio of the finite element mesh and increased the accuracy of the solution.

3. Results

3.1. Induced current density in a Petri dish containing only cell culture medium

The magnitude and spatial distribution of the induced electric field (E) and current density (J) in a 35 mm diameter Petri dish containing cell culture medium, placed in the central plane between the Helmholtz coils were computed. The computed values of J and E increased from zero at the centre of the Petri dish to a maximum of 2.4 mA m⁻² and 1.6 mV m⁻¹, respectively, at the edge of the dish. These results were within 1.6% of the analytical solution for the induced E and J in a cell culture medium exposed to a uniform time-varying MF (Chatterjee *et al* 2001). Although the computations were performed for a magnetic flux density of 5 Gauss, the results can be scaled linearly for other applied magnetic flux densities.

3.2. J in the vicinity of a single spherical chromaffin cell

Figure 3(a) shows a contour plot of the computed magnitude and spatial distribution of J in a Petri dish containing cell culture medium and a single spherical cell. J was plotted in the x - y ($z = 0$) plane passing through the centre of the cell. In the immediate vicinity of the cell, the magnitude of J deviated substantially from the value (0.85 mA m⁻²) computed in the absence of the cell. At the equator of the cell, there was a 50% increase in J , whereas at the poles, there was a 50% decrease. (In this figure and in all subsequent figures, the equator is defined as the direction perpendicular to the induced current while poles are defined as the direction parallel to the induced current.) Similar patterns of J were obtained at different z coordinates. However, the values of the maximum J decreased upon moving from the central x - y -plane. These findings indicate that a single spherical cell is exposed to different values of J along the z -axis. Figure 3(b) is an arrow plot of J in the central x - y -plane illustrating the

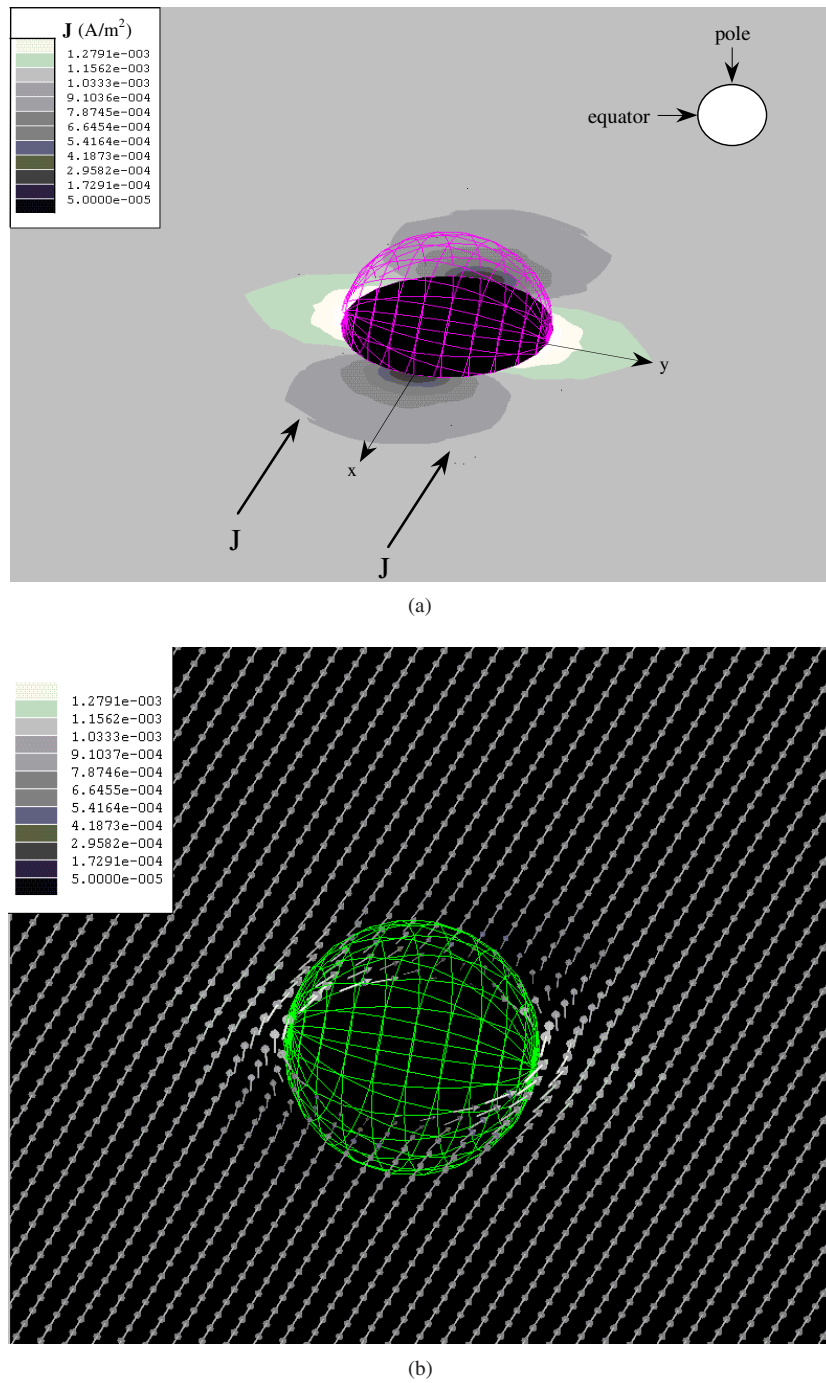


Figure 3. The magnitude and spatial distribution of J (plotted in the central x - y -plane) in the immediate vicinity of a single chromaffin cell exposed to a 5 Gauss magnetic flux density. Induced J is parallel to the x -axis and the inset indicates the locations of the equator (where maxima occur) and the poles (where minima occur). The centre of the cell is 6 mm from the centre of the dish. (a) Contour plot and (b) arrow plot showing the direction of induced current flow around the cell.

direction of induced current flow around the cell. The current bifurcated when it encountered the insulating cell membrane and flowed around the cell. A similar current flow path was observed in all cutplanes parallel to the central x - y -plane.

3.3. J in the vicinity of two or more spherical chromaffin cells separated by various distances

3.3.1. Two cells placed along the same radial line. Figure 4(a) shows the contour plot of the magnitude and spatial distribution of J in the vicinity of two chromaffin cells located at different distances from the centre of the dish but along the same radial line. Cells were separated by a distance of $10\ \mu\text{m}$ (equivalent to the cell radius). Maxima and minima, similar to those observed for single cells, occurred at the farthest equatorial sides and poles respectively, for each cell. However, there was a 60% increase (relative to the value in the absence of cells) in the maximum value of J in the equatorial region between the cells (i.e. along the y -axis). This indicated that J was more enhanced along the equatorial region between the cells than at the far equatorial sides of the cells. Similar patterns of J were observed at different z coordinates. However, the values of the maximum J in the region between the cells decreased upon moving from the central x - y -plane, where the distance between the cell centres was $10\ \mu\text{m}$, towards the poles where the distance between the cell centres was $30\ \mu\text{m}$ apart.

3.3.2. Two cells placed at the same radial distance from the centre of the Petri dish.

Figure 4(b) shows the magnitude and spatial distribution of J in the central x - y -plane in the vicinity of two chromaffin cells separated by a distance of $10\ \mu\text{m}$ and each placed at the same radial distance from the centre of the Petri dish. In this configuration, the maximum value of J located at the equatorial sides of the cells was the same as that computed for a single cell. In the region between the poles of the two cells, the value of J showed only a minimal difference (an increase of 1%) over the value computed for a single cell and was thus affected less than when cells were placed along the same radial line.

3.3.3. Effect on J due to the proximity of neighbouring cells. Computations were performed in which the distance between two cells was gradually increased from $10\ \mu\text{m}$ (equivalent to half a cell diameter) to $80\ \mu\text{m}$ (equivalent to four cell diameters). When the cells were placed along the same radial line (as in figure 4(a)), the maximum value of J between the cells decreased as the distance between the cells in the y -direction increased. These data are shown in figure 5. At a distance of approximately $60\ \mu\text{m}$, which was equivalent to three cell diameters, there was no longer a significant effect on J due to the presence of a neighbouring cell and the maximum of J was similar in magnitude to that observed for a single cell.

When two cells were placed at the same radial distance from the centre of the Petri dish (as in figure 4(b)) and the distance between the cell centres increased, the small change (1% increase over the value computed for a single cell) in the minimum value of J was absent once the distance between the poles of the cells reached $60\ \mu\text{m}$ (data not shown). Thus, in both configurations, when the distance between the cells was approximately three cell diameters or more, the value of J was the same as when the cells were isolated.

To examine the effect on J due to the presence of several equidistant neighbouring cells, four spherical cells were placed at equal distances of $60\ \mu\text{m}$ (three cell diameters) from a central cell (figure 6). The magnitude and spatial distribution of J in the vicinity of each of the five cells were almost identical to those that would be present for each of the five cells in the absence of the neighbouring cells. These results again showed that when the distances between several neighbouring spherical cells were approximately three cell diameters or more, the value of J was the same as when the cells were isolated.

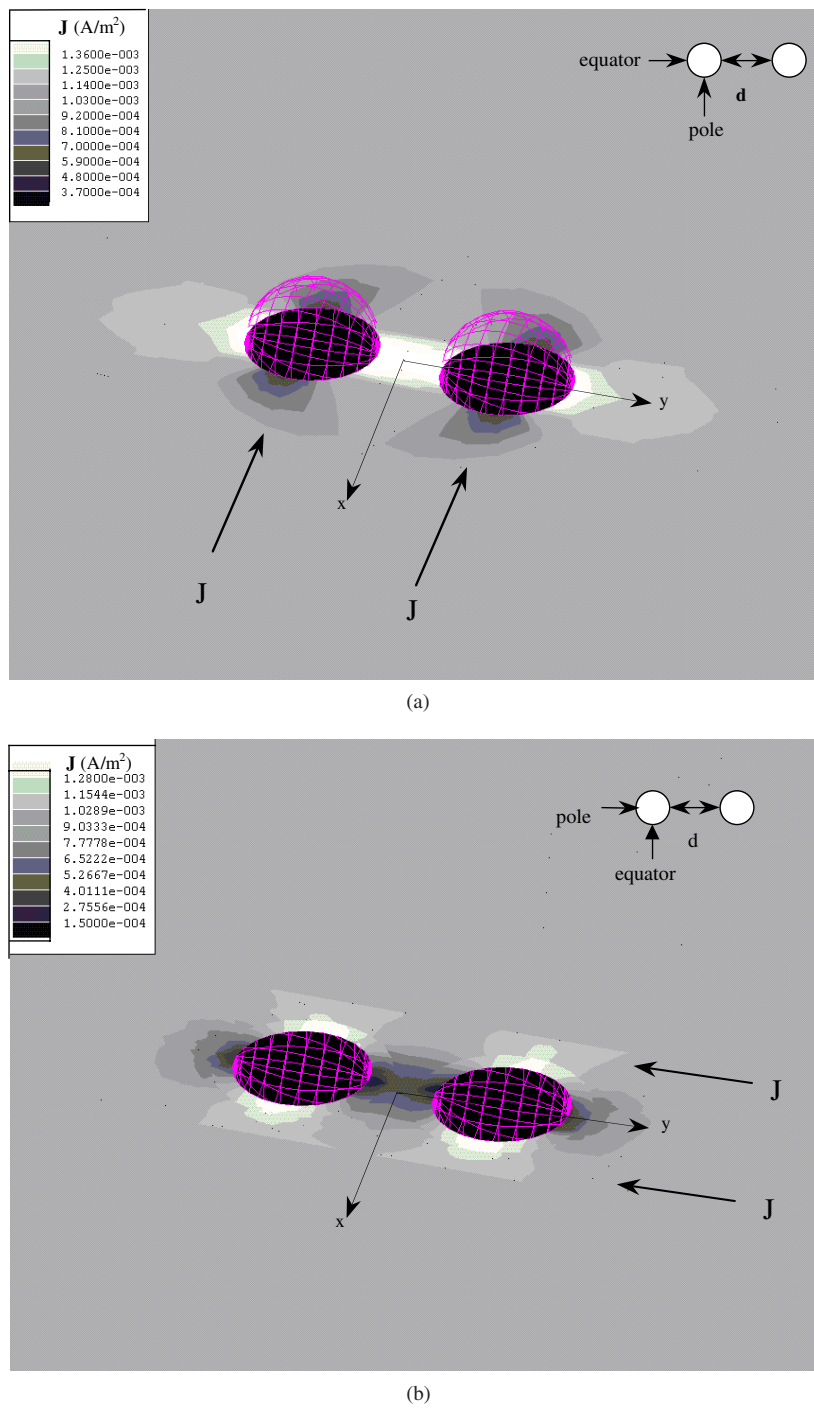


Figure 4. Contour plot of the magnitude and spatial distribution of J (plotted in the central x - y -plane) in the region occupied by two chromaffin cells separated by a distance $d = 10 \mu\text{m}$. The midpoint of the line joining the cell centres is 6 mm from the centre of the dish. (a) Cells are placed on the same radial line. Induced J direction is parallel to the x -axis. (b) Cells are at the same radial distance. Induced J direction parallel to the y -axis. Equators and poles are shown in the inset.

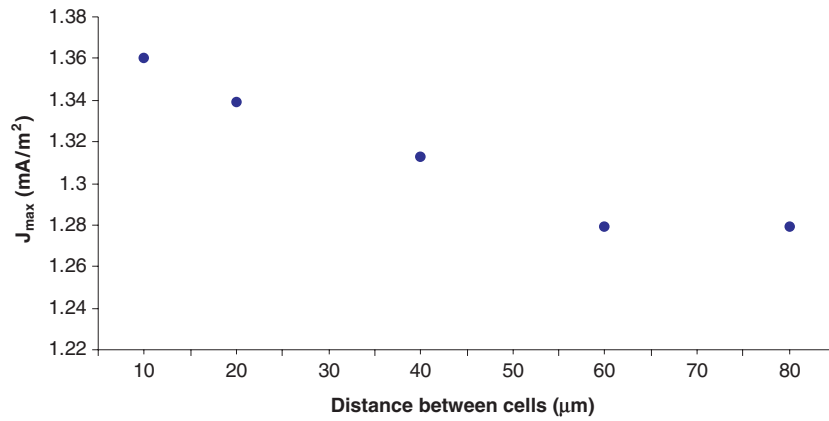


Figure 5. Maximum value of J in the region between two chromaffin cells as a function of the distance between the two cells.

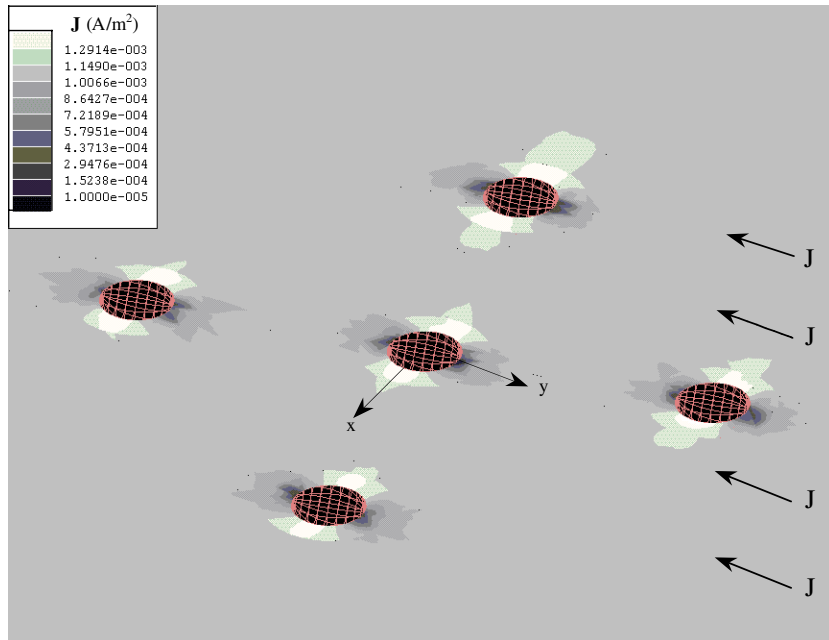
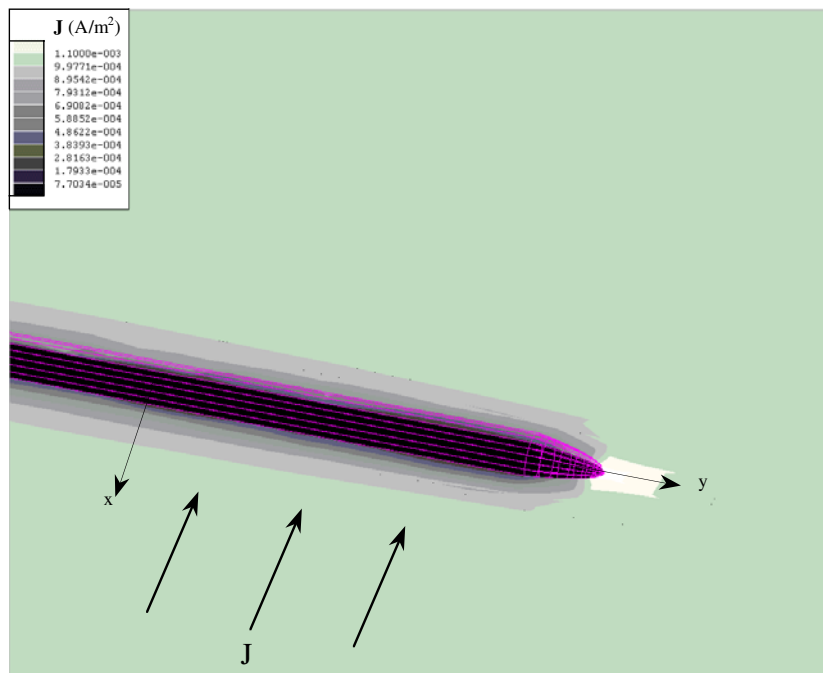


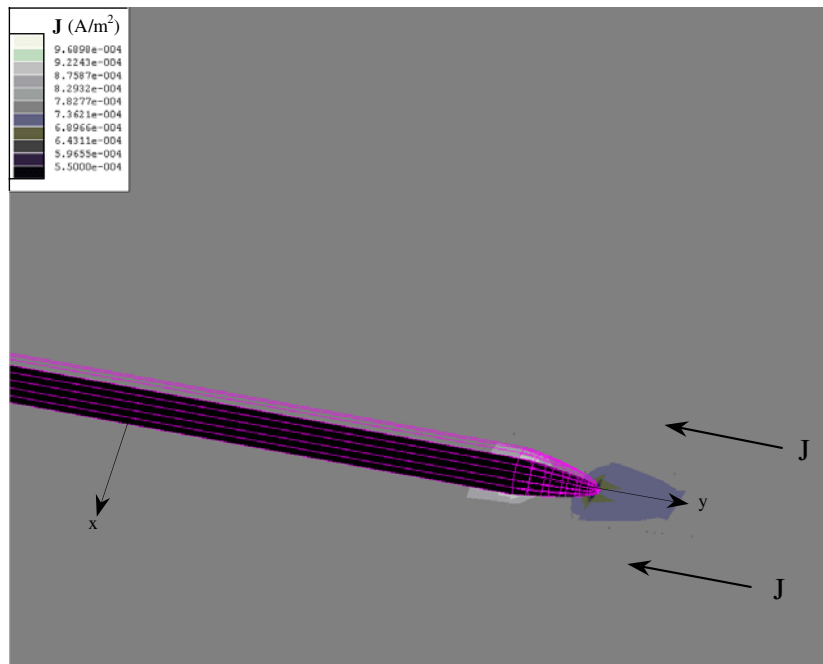
Figure 6. Contour plot of the magnitude and spatial distribution of J (plotted in the central x - y -plane) in the immediate vicinity of five chromaffin cells. J is parallel to the y -axis. Equators of the cells (where maxima occur) are located along the x -axis, while poles (where minima occur) are located along the y -axis.

3.4. J in the vicinity of an elongated smooth muscle cell modelled as a cylinder with smooth tapered end caps

Figure 7 shows contour plots of the magnitude and spatial distribution of J around a realistic model of a single smooth muscle cell, represented by a cylinder with smooth tapered end caps. For better visualization of the perturbations in J , only part of the cell is shown. Two orientations of J with respect to the long axis of the cell were modelled.



(a)



(b)

Figure 7. Contour plot of the magnitude and spatial distribution of J (plotted in the central x - y -plane) in the immediate vicinity of an elongated cell: (a) J is perpendicular to the long axis of the cell and (b) J is parallel to the long axis of the cell.

3.4.1. J perpendicular to the long axis of the cell. In this orientation, maxima in J (a 28% increase from the unperturbed value in the absence of the cell) occurred at the tapered ends of the cell while minima in J (a 50% decrease from the unperturbed value) occurred along the length of the cell parallel to the y -axis (figure 7(a)). Maxima and minima in J were also observed in various z -planes parallel to the central x - y -plane ($z = 0$ at the central plane to $z = \pm 2.5 \mu\text{m}$ at the poles of the cells) but the values were less than those in the central x - y -plane. This finding suggests that an elongated cell, as well as a spherical cell, is exposed to different values of J in the central x - y -plane as well as in cutplanes parallel to it. Also, as is the case for a spherical cell (shown earlier figure 3(b)), current flowed around the cell rather than through the high resistivity membrane (data not shown).

3.4.2. J parallel to the long axis of the cell. In this orientation, there was a minor effect on J (a decrease of 1% from the unperturbed value) at the very tip of the end caps, while an 8% increase in J occurred at the location where the cylinder begins to taper (figure 7(b)). No perturbations were observed along the length of the cell along the y -axis. In addition, spatial variations in J were similar in various z -planes parallel to the central x - y -plane. Thus, small perturbations in J were present only at the tapered part of the cell with no perturbations along the length of the cell or in cutplanes parallel to it.

3.5. J in the vicinity of a chain of spherical chromaffin cells

Chromaffin cells in culture can aggregate as chains of cells. Typically, the regions of contact tend to be fairly large giving the cells a flattened appearance in these regions, as shown in the inset of figure 8, where the magnitude and distribution of J in the vicinity of a chain of six chromaffin cells are shown. Here J is parallel to the long axis of the chain. For better visualization of the results, only three cells in one half of the chain are shown, the results being symmetrical for the three cells in the other half of the chain. Maxima were observed at the equatorial sides of each cell (along the x -axis), and minima at the poles (along the y -axis). In addition, local minima in J were observed in the vicinity of regions of contact between cells. As expected, there was no current flow due to the high resistivity cell membranes in regions where the cells were in contact. However, in cutplanes parallel to the central x - y -plane, current flowed in the regions between the cells.

Thus, in contrast to an elongated smooth muscle cell with its long axis parallel to J where there were no perturbations in J along the length of the cell (figure 7(b)), significant perturbations in J occurred along the length of a chain of spherical cells. On the other hand, when J was perpendicular to the long axis of the chain of cells, a pattern of J similar to that of an elongated cell (figure 7(a)) was observed (data not shown).

3.6. J in the vicinity of irregularly shaped aggregates of spherical chromaffin cells

Figures 9(a) and (b) show the magnitude and spatial distribution of J in the vicinity of a realistic chromaffin cell aggregate consisting of three cells for two orientations of the induced current density relative to the spatial position of the cells in the aggregate. The insets show the position of each cell within the aggregate. Looking at the aggregate as a whole, when J was parallel to the x -axis (figure 9(a)), a maximum increase in J of approximately 50% from the unperturbed value was observed at the equatorial sides of the aggregate (along the y -axis). Minima were also observed at the poles of the aggregate (along the x -axis) as well as in the vicinity of the regions where the cells made contact (along the y -axis). Similarly, when J was parallel to the y -axis (figure 9(b)), minima and maxima were observed at the poles and

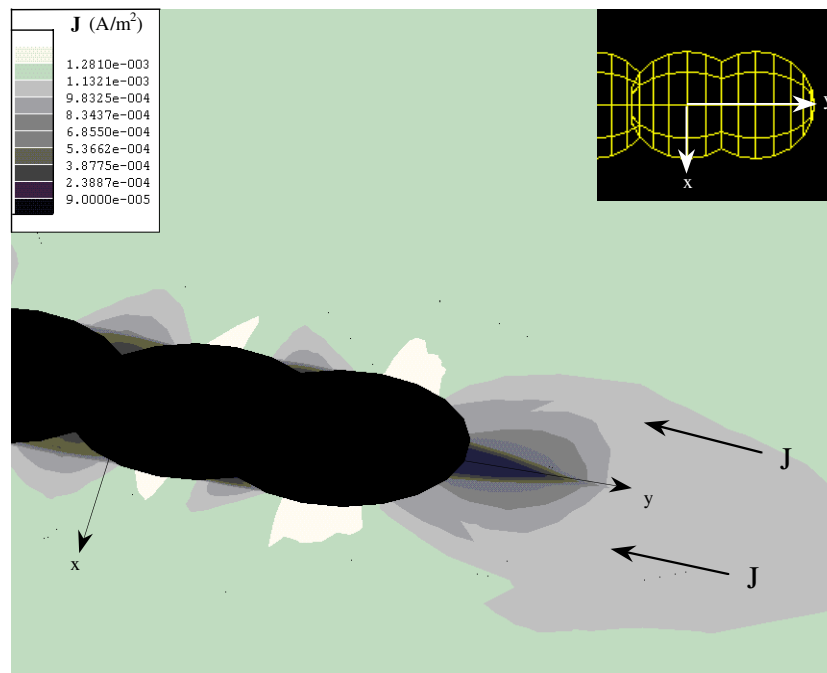


Figure 8. Contour plot of the magnitude and spatial distribution of J (plotted in the central x - y -plane) in the immediate vicinity of a realistic long chain of six chromaffin cells. J is parallel to the long axis of the chain. The inset shows a top view of the geometry of the cell chain.

equatorial sides of the aggregate respectively. However, in the vicinity of the region where cells 1 and 2 made contact, a local minimum (along the x -axis) was present between the two maxima at the equatorial sides of these cells. Similar to some of the previously described cases (e.g., single chromaffin cell, two chromaffin cells in close proximity to each other, elongated smooth muscle cell), each cell in the aggregate was exposed to different values of J along the z -axis. As z increased from zero at the central x - y -plane to $\pm 10 \mu\text{m}$ at the poles, the cell boundaries were farther apart and current was able to flow in regions where the cells were not in direct contact.

For a larger irregularly shaped realistic aggregate of six cells (figure 10), the spatial distribution of J was highly dependent on the spatial position of each cell and the regions of cell contact relative to the individual J . Distinct maxima were obtained at the equatorial sides, and minima at the poles of the aggregate as well as local minima in the vicinity of regions of contact between cells. These results were similar to those obtained for the smaller aggregate of three cells (figure 9(b)).

4. Discussion and conclusions

Studies examining the effects of applied time-varying MFs on cells in culture are usually designed to ensure the presence of uniform MFs in the region where a culture dish is placed during the exposures. However, little is known about how the very presence of the cells being exposed can perturb the uniformity of the induced currents and E -fields. This paper addresses this issue by providing a detailed description and quantification of the perturbations in the magnitude and spatial distribution of 60 Hz MF-induced currents in the immediate vicinity of

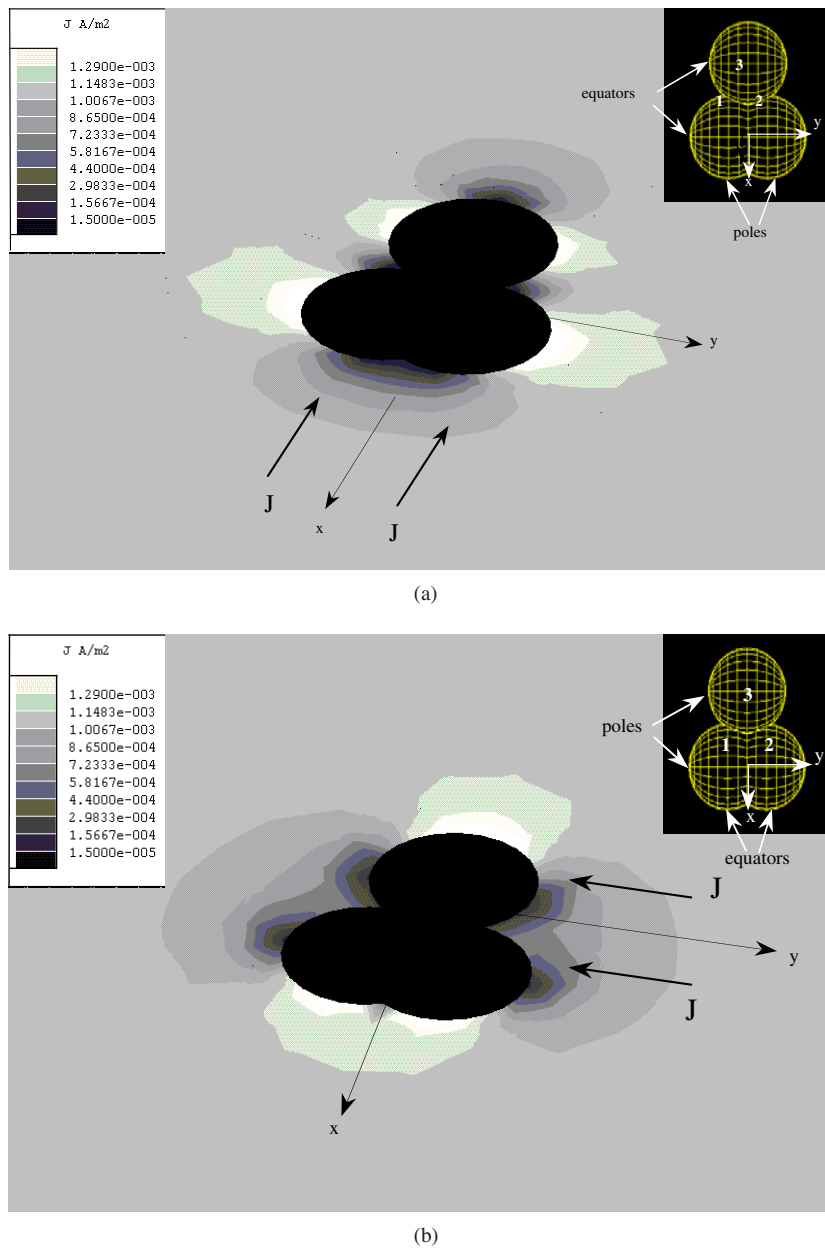


Figure 9. Contour plot of the magnitude and spatial distribution of J (plotted in the central x - y -plane) in the immediate vicinity of a small realistic aggregate of three chromaffin cells in the central x - y -plane: (a) J parallel to the x -axis and (b) J parallel to the y -axis. The insets show a top view of the cell aggregate.

realistic isolated cells and cell aggregates. Several parameters that were found to affect the distribution of the induced current in the vicinity of the cells are listed in table 2 and include cell and cell aggregate shape, spatial position of individual cells in the Petri dish, proximity

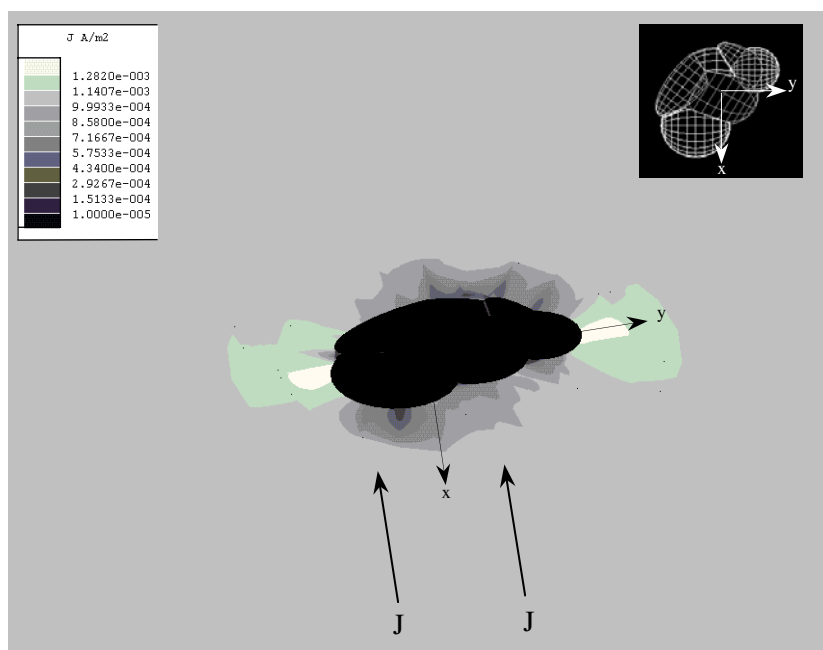


Figure 10. Contour plot of the magnitude and spatial distribution of J (plotted in the central x - y -plane) in the immediate vicinity of a realistic cell aggregate of six chromaffin cells. The direction of J , equators and poles of the aggregate as a whole are the same as in figure 4(a). The inset shows a top view of the arrangement of the six cells in the aggregate.

of neighbouring cells, and, position and orientation of cells within an aggregate with respect to the induced current density.

Regarding the effect of cell shape on the induced J , perturbations are more pronounced for spherical cells than for elongated cells. Moreover, elongated cells positioned with their long axis parallel to the induced J produce less perturbation than when positioned with their long axis perpendicular to the induced J . These findings demonstrate the significance of cell shape in determining the magnitude and spatial distribution of the current induced in realistic cell preparations exposed to 60 Hz MFs. They also show that for certain cell shapes, perturbations in the induced J can be further influenced by the orientation of the cells relative to the induced E -field. The physiological relevance of this latter finding is apparent in the study by Lee and McLeod (2000), which showed that the morphology of osteoblast-like cells exposed to 60 Hz MFs differs according to cell orientation. Cells oriented parallel to the induced E -field are significantly shorter and more circular than cells positioned perpendicular to the induced E -field.

When spherical cells are present as a chain parallel to the induced J in the dish, the perturbations in induced J do not equate with those for a similarly positioned elongated cell. There are significant perturbations along the length of the chain whereas perturbations along the length of the elongated cell are insignificant. On the other hand, the perturbations in both cases are very similar when each is oriented perpendicular to the induced J . These results emphasize the importance of (1) using realistic geometries (i.e., individual cells) rather than a simplified shape such as a cylinder for accurately assessing spatial distributions in the induced J in the vicinity of a chain of cells and, (2) noting, as for an elongated cell, the orientation of the chain of cells with respect to the direction of the induced E -field or induced J .

Table 2. Parameters affecting the induced current density in the vicinity of single cells and cell aggregates and a brief summary of the effects.

Parameter	Effect
Cell shape	Significant perturbations produced by: <ul style="list-style-type: none"> • a single spherical cell • a single elongated cell perpendicular to E
Orientation with respect to the induced E -field	Perturbations: <ul style="list-style-type: none"> • greater for an elongated cell with long axis perpendicular to E than when parallel to E; • significant both when the long axis of a spherical cell chain is perpendicular and parallel to E
<i>For spherical cells only</i>	
Spatial position of cells relative to the centre of a culture dish	Perturbations: more pronounced when cells are located along the same radial line than at the same radial location
Proximity of cells to each other	Perturbations produced by isolated cells: greater when a neighbouring cell(s) is within three cell diameters
Cell aggregates	Perturbations: <ul style="list-style-type: none"> • are more pronounced for a chain of cells than for a comparably-sized single elongated cell; • are quite pronounced and complex for irregularly shaped aggregates

Culture dishes containing non-confluent monolayers of spherical cells typically have a random spatial distribution of single cells and also cells in aggregates, as in the case of cultured chromaffin cells. Our results provide insight into how such arrangements of cells affect the induced J . For the simple case where two spherical cells do not touch each other, the perturbations in induced J produced by each cell can vary in magnitude in the region between the cells. These variations are a function of both the spatial location of the cells in the Petri dish and the distance of the cells from each other. Specifically, the perturbations are greater when the two cells are positioned along the same radial line but at different distances from the centre of the Petri dish, than when the two cells are located at the same radial distance from the centre of the Petri dish. This influence of neighbouring cells on the magnitude of the perturbations in induced J between the cells is lost once the distance separating the cells reaches approximately three cell diameters. These findings also apply to the more complex situation where many single spherical cells are present and not touching.

When spherical cells are instead touching and present in both small and large aggregates, both the spatial position of each cell in the aggregate and the regions of cell contact, relative to the direction of the induced J , affect the magnitude of the perturbations in J . In the case where spherical cells are present in a chain and the entire length of the chain is oriented parallel to the induced J , there will be maxima and minima at the equatorial sides and poles, respectively, and also local minima in the vicinity of the regions of contact between cells. When segments of the chain are not oriented parallel to the induced J , the pattern of the perturbations in the current density will therefore be different along the length of the chain. In the case where cells are present in irregularly shaped aggregates, the distribution of J is also affected in a complex manner that depends on how the individual cells in the aggregate are positioned relative to

their neighbours as well as with respect to the induced E (or J). Consequently, the magnitude of the perturbations will vary and either increases or decreases will be manifested.

Although our numerical modelling data describe only the induced E -fields and current densities external to the excitable cell models used in this study, future studies will be important for extending our findings to include the determination of how specific cellular processes in these and other excitable cells are impacted by the perturbations in the induced J . Nevertheless, at the present time we can make some predictions regarding possible physiological impact. For example, MF induced E -fields might be sufficient to influence electric charges and hence activity of membrane proteins located on or near the plasma membrane. Proteins such as receptors for growth factors and neurotransmitters, as well as ion channels, are sensitive to local charge distribution. The spatial distribution of an induced J around single cells and individual cells in aggregates, as well as the amount of exposed charge on a cell could therefore have direct bearing on the extent to which cellular responses occur. A case in hand is the secretory response of chromaffin cells. Because the release of catecholamines from these cells is polarized (Cuchillo *et al* 1999), only certain patterns of induced current may be capable of influencing plasma membrane proteins on the side of the cell where release primarily occurs and thus cause a secretory response.

In conclusion, taking into account the parameters that this study has identified as affecting the distribution of MF induced J in the vicinity of cells contained in a culture dish should help to provide a framework upon which responses of the cells to ELF-MF exposure can be better assessed. This will be particularly important for interpreting the experimental results of MF exposure studies as well as for efforts of researchers attempting to replicate their own findings and those of other laboratories. The results of this study may also shed light on the mechanisms underlying cellular effects of directly applied ELF E -fields that are reported to be governed by cell shape (Lee and McLeod 2000) and cell density (McLeod *et al* 1993a, b). Ultimately, we hope to gain insight into how MF-induced E -fields can be applied to target specific cellular processes at the whole tissue level and thus better predict potential clinical uses of MFs.

Acknowledgments

This research was supported by grants from NIEHS (RO1 ES07563) and an NSF EPSCoR cooperative agreement (OSR 9353227).

References

- Bassen H, Litovitz T, Penafiel M and Meister R 1992 ELF in vitro exposure system for inducing uniform electrical and magnetic fields in cell culture medium *Bioelectromagnetics* **13** 183–98
- Chatterjee I, Hassan N, Craviso G L and Publicover N G 2001 Numerical computation of distortions in magnetic fields and induced currents in physiological solutions produced by microscope objectives *Bioelectromagnetics* **22** 463–9
- Craviso G L, Poss J, Lanctot C, Lundback S S, Chatterjee I and Publicover N G 2002 Intracellular calcium activity in isolated bovine adrenal chromaffin cells in the presence and absence of 60 Hz magnetic fields *Bioelectromagnetics* **23** 557–67
- Cuchillo I, Michelena P, Albillos A and Garcia A G 1999 A preferential pole for exocytosis in cultured chromaffin cells revealed by confocal microscopy *FEBS Lett.* **459** 22–6
- Foster K R and Schwan H P 1989 Dielectric properties of tissues and biological materials: a critical review *CRC Crit. Rev. Biomed. Eng.* **17** 25–104
- Goodman E M, Greenebaum B and Marron M T 1995 Effects of electromagnetic fields on molecules and cells *Int. Rev. Cytol.* **158** 279–338

- Goodman R and Henderson A S 1991 Transcription and translation in cells exposed to extremely low frequency electromagnetic fields *Bioelectrochem. Bioenerg.* **25** 335–55
- Graham C, Cook M R, Cohen H D and Gerkovich M M 1994 Dose response study of human exposure to 60 Hz electric and magnetic fields *Bioelectromagnetics* **15** 447–63
- Hart F X 1996 Cell culture dosimetry for low frequency magnetic fields *Bioelectromagnetics* **17** 48–57
- Hassan N, Chatterjee I, Publicover N G and Craviso G L 2002 Mapping membrane potential perturbations of chromaffin cells exposed to electric fields *IEEE Transac. Plasma Sci.* **30** 1–9
- Kanje M, Rusovan A, Sisken B and Lundborg G 1993 Pretreatment of rats with pulsed electromagnetic fields enhances regeneration of the sciatic nerve *Bioelectromagnetics* **14** 353–9
- Kato M, Honma K, Shigemitsu T and Shiga Y 1994 Circularly polarized 50-Hz magnetic field exposure reduces pineal gland and blood melatonin concentrations of Long-Evans rats *Neurosci. Lett.* **17**, **166** 59–62
- Lee J H and McLeod K J 2000 Morphologic responses of osteoblast-like cells in monolayer culture to ELF electromagnetic fields *Bioelectromagnetics* **21** 129–36
- Liburdy R P 1995 Cellular studies and interaction mechanisms of extremely low frequency fields *Radio Sci.* **30** 179–202
- Luben R A 1991 Effects of low energy electromagnetic fields on membrane signal transduction processes in biological systems *Health Phys.* **61** 15–28
- Maxwell 3D Field Simulator User's Reference 1993 Ansoft Corporation, Pittsburgh, PA
- McLeod K J, Donahue H J, Levin P E, Fontaine M-A and Rubin C T 1993a *J. Bone Miner. Res.* **8** 977–84
- McLeod K J, Donahue H J, Fontaine M-A and Rubin C T 1993b Cell density effects on the interaction of electric fields with cells in vitro *Electricity and Magnetism in Biology and Medicine* (San Francisco, CA: San Francisco Press) pp 291–4
- McLeod B R, Pilla A A and Sampsel M W 1983 Electromagnetic fields induced by Helmholtz aiding coils inside saline filled boundaries *Bioelectromagnetics* **4** 357–70
- Misakian M and Kaune W T 1990 Optimal experimental design for *in vitro* studies with ELF magnetic fields *Bioelectromagnetics* **11** 251–5
- Misakian M, Sheppard A R and Krause D 1993 Biological, physical and electrical parameters for in-vitro studies with ELF magnetic and electric fields: a primer *Bioelectromagnetics* suppl 2 1–74
- Morgan N G 1989 *Cell Signaling* (New York: The Guilford Press)
- Pilla A A 1993 State of the art in electromagnetic therapeutics *Electricity and Magnetism in Biology and Medicine* (San Francisco, CA: San Francisco Press) pp 17–22
- Polk C 1990 Electric field and surface charges induced by ELF magnetic fields *Bioelectromagnetics* **11** 189–201
- Stuchly M A and Xi W 1994 Modelling induced currents in biological cells exposed to low frequency magnetic fields *Phys. Med. Biol.* **39** 1319–30
- Tenforde T S 1991 Biological interactions of extremely low frequency electric and magnetic fields *Bioelectrochem. Bioenerg.* **25** 17
- Tenforde T S 1993 Cellular and molecular pathways of extremely-low-frequency electromagnetic field interactions with living systems *Electricity and Magnetism in Biology and Medicine* (San Francisco, CA: San Francisco Press) pp 1–8
- Tenforde T S 1996 Interaction of ELF magnetic fields with living systems *Biological Effects of Electromagnetic Fields* (Boca Raton, FL: CRC Press) pp 185–230
- Ueno S, Tashiro T and Harada K 1988 Localized stimulation of neural tissues in the brain by means of a paired configuration of time-varying magnetic fields *J. Appl. Phys.* **64** 5862–4
- Wertheimer N and Leeper E 1979 Electrical wiring configurations and childhood cancer *Am. J. Epidemiol.* **109** 273–84